

Two-fluid Instability of Dust and Gas in the Dust Layer of a Protoplanetary Disk

Naoki Ishitsu¹, Shu-ichiro Inutsuka² and Minoru Sekiya¹

ishitsu@geo.kyushu-u.ac.jp

ABSTRACT

Instabilities of the dust layer in a protoplanetary disk are investigated. It is known that the streaming instability develops and dust density concentration occurs in a situation where the initial dust density is uniform. This work considers the effect of initial dust density gradient vertical to the midplane. Dust and gas are treated as different fluids. Pressure of dust fluid is assumed to be zero. The gas friction time is assumed to be constant. Axisymmetric two-dimensional numerical simulation was performed using the spectral method. We found that an instability develops with a growth rate on the order of the Keplerian angular velocity even if the gas friction time multiplied by the Keplerian angular velocity is as small as 0.001.

This instability is powered by two sources: (1) the vertical shear of the azimuthal velocity, and (2) the relative motion of dust and gas coupled with the dust density fluctuation due to advection. This instability diffuses dust by turbulent advection and the maximum dust density decreases. This means that the dust concentration by the streaming instability which is seen in the case of a uniform initial dust density becomes ineffective as dust density gradient increases by the dust settling toward the midplane.

Subject headings: planetary systems: protoplanetary disks—solar system: formation—hydrodynamics—instabilities

1. INTRODUCTION

The first step for planetary formation requires the formation of planetesimals larger than km-size. However, the mechanism that planetesimals are formed from dust is scarcely understood. The two different paths to planetesimal formation have been studied. The one is the discontinuous formation due to the gravitational instability of the dust layer (Safronov 1969; Goldreich & Ward 1973; Coradini et al. 1981; Sekiya 1983; Yamoto & Sekiya 2004; Wakita & Sekiya 2008). The other

¹Department of Earth and Planetary Sciences, Faculty of Sciences, 33 Kyushu University, Hakozaki, Fukuoka, 812-8581, Japan

²Department of Physics, Nagoya University, Furocho, Nagoya, Aichi 464-8602, Japan

one is the continuous growth to planetesimals due to the sticking (Weidenschilling & Cuzzi 1993; Cuzzi et al. 1993; Wurm et al. 2001; Kornet et al. 2001).

The gravitational instability has advantage because the problem that meter-sized dust falls toward a central star is avoided. The gravitational instability is theoretically more tractable because the formation process dose not depend on poorly-understood surface forces of dust material. However, if the disk is turbulent, the critical density for the gravitational instability cannot be reached because the dust is stirred from the midplane. The magneto rotational instability (MRI) is a candidate for turbulent sources in the stage of the planet formation (Balbus & Hawley 1991). The ionization degree is so low in the planet forming region that there is possibility that the MRI does not occur there (Sano et al. 2000). It is pointed that the dust layer can become turbulent because of the shear instability even if the global turbulence such as MRI does not occur (Weidenschilling 1980). The shear instability has been extensively studied analytically (Sekiya 1998; Sekiya & Ishitsu 2000, 2001; Ishitsu & Sekiya 2002, 2003; Michikoshi & Inutsuka 2006) and numerically (Cuzzi et al. 1993; Dobrovolskis, Dacles-Mariani, & Cuzzi 1999; Johansen et al. 2006b; Chiang 2008; Barranco 2009).

Recently, a different type of instability in the dust layer draws attention. The gas supported by a negative radial pressure gradient revolves slower than the Kepler velocity. The dust revolves against the head wind. As a result, the dust falls toward the central star by losing the angular momentum (Adachi et al. 1976; Weidenschilling 1977). On the other hand, the gas moves outward in the disk by gaining the angular momentum (Nakagawa et al. 1986). Youdin & Goodman (2005) has found the streaming instability can occur when dust and gas have relative velocities. Furthermore, Youdin & Johansen (2007) and Johansen & Youdin (2007) have detailedly performed analysis and numerical simulations on the streaming instability in the situation that the unperturbed dust density is spatially homogeneous and the gravity in the axial direction of rotation is ignored. The simulations showed that the streaming instability has the action which concentrates dust. Johansen et al. (2007) has presented that Ceres-sized planetesimals are formed by the dust concentration due to the streaming instability and the self-gravity when there are meter-sized boulders in the MRI turbulence disk. However, the concentration by the streaming instability is only effective for dust larger than 10cm in size. It is not known whether dust can grow up to this size.

It has been yet to be studied what instability occurs when the dust has distribution with a vertical gradient. It is important to examine instability in this case in order to understand the growth of dust. In this work, we perform two-fluid of gas and dust with a single size, two-dimensional simulations. We present that instability occurs and flow transits into turbulence if dust with cm-sized has a graded density distribution.

In §2, the formulation is performed under assumptions of the fluid approximation of gas and dust. In §3, numerical results are presented. In §4, we discuss the energy sources of instability by deriving energy equations from linearized equations. In §5, we conclude.

2. BASIC EQUATIONS

This section gives the basic equations. The gas friction force is characterized by the friction time τ_f , which is the time during which the relative velocity of a dust aggregate and the gas becomes $1/e$. The friction time depends on the radius of dust aggregate a , the dust solid density ρ_s , the gas density ρ_g , and the thermal velocity c_{th} . In the Hayashi model, the friction time is given Epstein's law (Epstein 1924) and Stokes' law (Landau & Lifshits 1987)

$$\tau_f \Omega_K = \left(1 + \frac{\pi}{8}\right) \frac{a \rho_s}{\rho_g c_{th}} \Omega_K = 1.19 \times 10^{-3} \left(\frac{\rho_s}{1 \text{gcm}^{-3}}\right) \left(\frac{a}{1 \text{cm}}\right) \left(\frac{r}{1 \text{AU}}\right)^{1.5} \text{ for } a \ll l_g, \quad (1)$$

$$\tau_f \Omega_K = \frac{2a^2 \rho_s}{3l_g c_{th}} \Omega_K = 2.77 \times 10^{-4} \left(\frac{\rho_s}{1 \text{gcm}^{-3}}\right) \left(\frac{a}{1 \text{cm}}\right)^2 \left(\frac{r}{1 \text{AU}}\right)^{-1.25} \text{ for } a \gg l_g, \quad (2)$$

where the mean free path of the gas is given by

$$l_g = \frac{1}{\sqrt{2} \rho_g / (\mu m_H) \sigma_{mol}} = 2.0 f_g^{-1} \left(\frac{r}{1 \text{AU}}\right)^{2.75} \text{ cm}, \quad (3)$$

where μ is the mean molecular weight, m_H is the mass of a hydrogen atom, and σ_{mol} is the mean cross section of the molecules, f_g is the gas density ratio compared to the Hayashi model (Hayashi 1981).

We assume that all dust aggregates have an identical friction time, and treat dust aggregates as a pressure-less fluid. The latter assumption is good only if $\tau_f \Omega_K \ll 1$ (Garaud & Lin 2004). However we performed numerical simulations for wide range of the value $\tau_f \Omega_K$ in order to understand basic physics of dust-gas two fluids.

We neglect the curvature of the cylindrical coordinates (r, ϕ, z) and use the local Cartesian coordinate system which rotates with the Keplerian velocity. Our coordinates x , y , and z denote radial, azimuthal, and vertical directions of the disk, respectively. That is, $x = r - R$, $y = R[\phi - \Omega_K(R)t]$, and z , where $\Omega_K(R)$ is the Keplerian angular velocity at a fiducial radius $r = R$ and we neglect higher order terms of x , y and z . In the following, we denote $v_K(R)$ and $\Omega_K(R)$ by v_K and Ω_K for simplicity. The gas can be assumed to be incompressible because the dust layer treated here is much thinner than vertical scale height of the gas disk and, in addition, the flow velocity is subsonic. The vertical components of the gravity of the central star and the disk self-gravity are neglected; this assumption is also used in the previous works (Youdin & Goodman 2005; Youdin & Johansen 2007; Johansen & Youdin 2007). We consider an unperturbed state in which the radial pressure gradient $\partial P_0 / \partial R$ is a negative constant.

We assume axisymmetric flows, i.e. physical quantities are independent of y . Thus, we obtain the continuity equations, the momentum equations of gas and dust,

$$\nabla_2 \cdot \mathbf{U}_g = 0, \quad (4)$$

$$\frac{\partial \mathbf{U}_g}{\partial t} + (\mathbf{U}_g \cdot \nabla_2) \mathbf{U}_g = -\frac{1}{\rho_g} \nabla_2 P - \frac{1}{\rho_g} \frac{\partial P_0}{\partial R} \hat{\mathbf{x}} + 2\mathbf{U}_g \times \boldsymbol{\Omega}_K + 3\Omega_K^2 x \hat{\mathbf{x}} - \frac{\rho_d}{\tau_f \rho_g} (\mathbf{U}_g - \mathbf{U}_d), \quad (5)$$

$$\frac{\partial \rho_d}{\partial t} + \nabla_2 \cdot (\rho_d \mathbf{U}_d) = \nu_D \nabla_2^2 \rho_d, \quad (6)$$

$$\frac{\partial \mathbf{U}_d}{\partial t} + (\mathbf{U}_d \cdot \nabla_2) \mathbf{U}_d = 2\mathbf{U}_d \times \boldsymbol{\Omega}_K + 3\Omega_K^2 x \hat{\mathbf{x}} - \frac{1}{\tau_f} (\mathbf{U}_d - \mathbf{U}_g), \quad (7)$$

where $\nabla_2 = (\frac{\partial}{\partial x}, 0, \frac{\partial}{\partial z})$, $\boldsymbol{\Omega}_K = (0, 0, \Omega_K)$, P is the local gas pressure perturbation, ρ_d is the dust density defined by the total dust mass floating in a unit volume, and $\mathbf{U} \equiv (U, V, W)$ is velocity of gas and dust, the subscripts g and d denote gas and dust, respectively. In order to solve the continuity equation of dust stably, the diffusive term is added to equation(6) artificially. The diffusive parameter ν_D is chosen so that the numerical stability is maintained, and also the numerical diffusion is negligibly small. We confirmed that dust mass was conserved in this method.

We perform velocity translation in the azimuthal direction following Johansen et al. (2006a). The system which balances between global pressure gradient, centrifugal force, and gravity at $r = R$ rotates with a sub-Kepler velocity given by

$$V_0 = -\frac{3}{2}\Omega_K x - \eta v_K, \quad (8)$$

where η is a dimensionless parameter which expresses the effect of global radial pressure gradient and defined by

$$\eta = -\frac{1}{2\rho_g \Omega_K^2 R} \frac{\partial P_0}{\partial R} = 1.81 \times 10^{-3} (R/1\text{AU})^{1/2}. \quad (9)$$

If the reaction force of dust on gas through the friction is negligibly small, the gas revolves at $\eta v_K = 54 \text{ m s}^{-1}$ slower than the Kepler velocity in the Hayashi model disk. Substituting $\mathbf{U} = \mathbf{u} - V_0 \hat{\mathbf{y}}$ into equations (4) – (7) gives

$$\nabla_2 \cdot \mathbf{u}_g = 0, \quad (10)$$

$$\frac{\partial \mathbf{u}_g}{\partial t} + (\mathbf{u}_g \cdot \nabla_2) \mathbf{u}_g = -\frac{1}{\rho_g} \nabla_2 P + 2\mathbf{u}_g \times \boldsymbol{\Omega}_K + \frac{3}{2} u_g \Omega_K \hat{\mathbf{y}} - \frac{\rho_d}{\tau_f \rho_g} (\mathbf{u}_g - \mathbf{u}_d), \quad (11)$$

$$\frac{\partial \rho_d}{\partial t} + \nabla_2 \cdot (\rho_d \mathbf{u}_d) = \nu_D \nabla_2^2 \rho_d, \quad (12)$$

$$\frac{\partial \mathbf{u}_d}{\partial t} + (\mathbf{u}_d \cdot \nabla_2) \mathbf{u}_d = 2\mathbf{u}_d \times \boldsymbol{\Omega}_K + \frac{3}{2} u_d \Omega_K \hat{\mathbf{y}} - \frac{1}{\tau_f} (\mathbf{u}_d - \mathbf{u}_g) - 2\eta v_K \Omega_K \hat{\mathbf{x}}. \quad (13)$$

Equations (10)–(13) are solved with the Fourier spectral method. Boundary conditions are periodic. As for periodic boundary condition of the z direction, computational box size L_z is large enough for dust not to cross the boundary and for the eigenfunction obtained by the normal mode analysis to decay. A second-order Adams-Bashforth scheme for the non-linear terms and a Crank-Nicolson scheme for the viscous terms are employed. We use the phase shift method to eliminate aliasing error (Canuto et al. 1988).

2.1. INITIAL CONDITIONS

Youdin & Goodman (2005), Youdin & Johansen (2007) and Johansen & Youdin (2007) investigated the streaming instability of the dust layer in a protoplanetary disk using an unstratified uniform dust density distribution as their initial conditions. However, a dust concentrated region in which the dust density has the same orders of magnitude with the gas density would be realized if dust settle toward the midplane, and the dust density should decrease with the distance from the midplane. As a simple model of this setting, we employ the initial density distribution which has constant dust density around the midplane and sinusoidal transition zones:

$$\rho_d(z) = \begin{cases} \rho_d(0) & \text{for } |z| \leq z_d - 2h_d, \\ \rho_d(0)\{1 - \sin[\pi(z - z_d + h_d)/2h_d]\}/2 & \text{for } z_d - 2h_d < |z| < z_d, \\ 0 & \text{for } z_d \leq |z|, \end{cases} \quad (14)$$

where z_d the half-thickness of the dust layer, and h_d the half-thickness of the transition zones, where the dust density varies from $\rho_{d0}(0)$ to 0 sinusoidally. Here the half-thickness of the dust layer is given by

$$z_d = \frac{\Sigma_d}{2\rho_d(0)} + h_d, \quad (15)$$

and the surface density of the dust is given by

$$\Sigma_d = \int_{-\infty}^{+\infty} \rho_d dz = \begin{cases} 7.1 f_d (r/\text{AU})^{-1.5} \text{ g cm}^2 & \text{for } r < 2.8\text{AU}, \\ 30 f_d (r/\text{AU})^{-1.5} \text{ g cm}^2 & \text{for } r > 2.8\text{AU}, \end{cases} \quad (16)$$

where f_d is a parameter ($f_d = 1$ for the Hayashi model). We used Hayashi's solar nebula model (Hayashi 1981; Hayashi et al. 1985) at 1AU as the dust surface density Σ_d . Initial velocities of dust and gas are given quasi-stationary flow obtained by Nakagawa et al. (1986).

$$\bar{u}_g = \frac{2\tau_f \Omega_K \rho_d \rho_g}{(\rho_d + \rho_g)^2 + (\tau_f \Omega_K \rho_g)^2} \eta v_K, \quad (17)$$

$$\bar{v}_g = \frac{\rho_d(\rho_d + \rho_g)}{(\rho_d + \rho_g)^2 + (\tau_f \Omega_K \rho_g)^2} \eta v_K, \quad (18)$$

$$\bar{u}_d = -\frac{2\tau_f \Omega_K}{(\rho_d + \rho_g)^2 + (\tau_f \Omega_K \rho_g)^2} \eta v_K, \quad (19)$$

$$\bar{v}_d = \left[1 - \frac{\rho_g(\rho_d + \rho_g)}{(\rho_d + \rho_g)^2 + (\tau_f \Omega_K \rho_g)^2} \right] \eta v_K, \quad (20)$$

$$\bar{w}_g = \bar{w}_d = 0. \quad (21)$$

Note that the co-ordinate system in this paper moves with sub-Kepler velocity $(1 - \eta)v_K$; on the other hand, it moves with the Kepler velocity v_K in Nakagawa et al. (1986).

3. NUMERICAL RESULTS

This section displays results of the numerical simulation of dust and gas, two-fluid simulations. Model parameters used in this work are listed in Table 1.

3.1. Constant Dust Density Distribution

We now present a simulation result under the constant dust distribution condition for comparing our work to Youdin & Johansen (2007) and Johansen & Youdin (2007). Figure 1 shows snapshots for the evolution of dust density, where $\rho_d(0)/\rho_g = 1$, $h_d/z_d = 0$, and $\tau_f\Omega_K = 1$. The streaming instability occurs similar to the results of Johansen & Youdin (2007). The dust concentration is seen after turbulence fully develops. Table 1 shows the growth rate ω_I and the radial wave number k of the most unstable mode. We performed the linear analysis based on Youdin & Johansen (2007), and confirmed that the streaming instability is reproduced well with an accuracy of 1 % error in the growth rate.

3.2. Stratified Dust Density Distribution

Here, results for stratified dust density distributions are presented. First, we investigate the case of $\tau_f\Omega_K = 10^{-3}$. This friction time corresponds to approximately 1cm dust diameter at 1 AU from equation (1). Figure 2 shows the initial profiles of the dust density and velocities of gas and dust for $\rho_d(0)/\rho_g = 1$ and $h_d/z_d = 0.5$. It is seen that the radial velocities of dust and gas are very slow, $|\bar{u}_g|/(\eta v_k), |\bar{u}_d|/(\eta v_k) \sim 10^{-3}$. Figure 3 shows snapshots of the evolution of dust density. The perturbation of short wave length grows by an instability, and the flow transits to turbulent state. And then, the dust is stirred from the midplane. Because the growth time of instability $1/\omega_I \sim 1\text{yr}$ is much shorter than the settling time of dust $1/(\tau_f\Omega_K^2) \sim 10^3\text{yr}$, the result would not change even if there is the vertical gravity which is omitted in our simulation. Thus, this instability may prevent the disk from the gravitational instability.

The dust concentration occurs as a result of “streaming instability” if the dust density distribution is constant as shown by Youdin & Goodman (2005), Youdin & Johansen (2007), and Johansen & Youdin (2007). However, if an initial dust density is not homogeneous, maximum dust density does not exceed initial one. The growth rate of instability is approximately the Keplerian frequency as seen in Table 1. The detail of the instability in this case is analyzed in §4. Figure 4 shows the evolution of r.m.s. of vertical dust velocities weight-averaged by dust density $\langle w_d \rangle_{rms}$. Here

$$\langle w_d \rangle_{rms} = \sqrt{\frac{\int \rho_d w_d^2 dV}{\int \rho_d dV}}. \quad (22)$$

The r.m.s of dust velocity shows the linear-growth at first and then saturates at $\langle w_d \rangle_{rms} \approx 0.1\eta v_K$

(several m/sec).

Next we consider the case of $\tau_f \Omega_K = 1$. This friction time approximately corresponds to dust with $a = 1\text{m}$ at 1AU from equation (2). In this case, we expect that the random velocities of dust is large, so that our approximation of pressure-less fluid for dust is not justified. However, we perform calculations for this case in order to understand the essence of the dust and gas two-fluid instability by comparing the results with that for $\tau_f \Omega_K = 10^{-3}$. Figure 5 shows the initial profiles of dust density and velocities of the gas and dust for $\rho_d(0)/\rho_g = 1$ and $h_d/z_d = 0.5$. A m-sized body falls toward a central star with velocity ηv_K . As the dust settles toward the midplane to form the dust layer, dust density grows compared with the gas density. Then, the infall velocity of dust toward the central star slows down due to the increase of dust inertia as seen from equation (19). On the other hand, gas moves outward by obtaining the angular momentum from dust as seen from equation (17). Radial velocities of dust and gas vary with the distance from midplane depending on the dust density; that is, the vertical shear of radial velocities arises. The density pattern of the shear instability is actually seen at the upper right panel in Figure 5. It is shown in §4 that the energy source of this instability is vertical shear of the azimuthal and radial components of the gas velocity.

The r.m.s. of a vertical dust velocity for $\tau_f \Omega_K = 1$ is two orders magnitude smaller than that for $\tau_f \Omega_K = 10^{-3}$ as seen in Figure 4. The reason would be that the coupling between gas and dust is weak. As shown by Johansen & Youdin (2007), dust concentrates by the streaming instability after the flow becomes turbulent. That is also seen in our simulation at $t\Omega_K = 26.5$ as shown in Figure 6.

In our calculation, the dust does not settle down because the gravity of central star is neglected. In reality, the dust would settle down before the start of the shear instability for the parameter, $\rho_d(0)/\rho_g = 1, h_d/z_d = 0.5$ and $\tau_f \Omega_K = 1$ because the settling time $1/(\tau_f \Omega_K^2) \sim 1/\Omega_K$ is shorter than the growth time of the turbulence. As dust settling proceeds, the shear instability occurs when the growth time of shear instability becomes shorter than the dust settling time (Johansen et al. 2006b; Johansen & Youdin 2007).

4. ENERGY SOURCES OF INSTABILITY

In this section, we analyze the energy source of the instabilities presented in §3. The energy budget for the instability can be estimated from distributions of density and velocities obtained by our simulations shown in §3.

4.1. Linearization

We linearize equations (10)–(13) as follows:

$$\frac{\partial u'_g}{\partial x} + \frac{\partial w'_g}{\partial z} = 0, \quad (23)$$

$$\frac{\partial u'_g}{\partial t} + \bar{u}_g \frac{\partial u'_g}{\partial x} + w'_g \frac{\partial \bar{u}_g}{\partial z} = -\frac{1}{\rho_g} \frac{\partial P'}{\partial x} + 2\Omega_K v'_g - \frac{1}{\tau_f \rho_g} \bar{\rho}_d (u'_g - u'_d) - \frac{1}{\tau_f \rho_g} \rho'_d (\bar{u}_g - \bar{u}_d), \quad (24)$$

$$\frac{\partial v'_g}{\partial t} + \bar{u}_g \frac{\partial v'_g}{\partial x} + w'_g \frac{\partial \bar{v}_g}{\partial z} = -\frac{1}{2} \Omega_K u'_g - \frac{1}{\tau_f \rho_g} \bar{\rho}_d (v'_g - v'_d) - \frac{1}{\tau_f \rho_g} \rho'_d (\bar{v}_g - \bar{v}_d), \quad (25)$$

$$\frac{\partial w'_g}{\partial t} + \bar{u}_g \frac{\partial w'_g}{\partial x} = -\frac{\partial P'}{\partial z} - \frac{1}{\tau_f \rho_g} \bar{\rho}_d (w'_g - w'_d). \quad (26)$$

$$\frac{\partial \rho'_d}{\partial t} + \bar{\rho}_d \frac{\partial u'_d}{\partial x} + \bar{u}_d \frac{\partial \rho'_d}{\partial x} + \bar{\rho}_d \frac{\partial w'_d}{\partial z} + \frac{\partial \bar{\rho}_d}{\partial z} w'_d = 0, \quad (27)$$

$$\frac{\partial u'_d}{\partial t} + \bar{u}_d \frac{\partial u'_d}{\partial x} + w'_d \frac{\partial \bar{u}_d}{\partial z} = 2\Omega_K v'_d - \frac{1}{\tau_f} (u'_d - u'_g), \quad (28)$$

$$\frac{\partial v'_d}{\partial t} + \bar{u}_d \frac{\partial v'_d}{\partial x} + w'_d \frac{\partial \bar{v}_d}{\partial z} = -\frac{1}{2} \Omega_K u'_d - \frac{1}{\tau_f} (v'_d - v'_g), \quad (29)$$

$$\frac{\partial w'_d}{\partial t} + \bar{u}_d \frac{\partial w'_d}{\partial x} = -\frac{1}{\tau_f} (w'_d - w'_g). \quad (30)$$

Assuming $f' \propto e^{i(kx - \omega t)}$ (k denotes the radial wave number, and $\omega = \omega_R + i\omega_I$ denotes the complex frequency), equations (23)–(30) are written as

$$iku'_g + \frac{dw'_g}{dz} = 0, \quad (31)$$

$$-i\tilde{\omega}_g u'_g + w'_g \frac{d\bar{u}_g}{dz} = -ik \frac{1}{\rho_g} P' + 2\Omega_K v'_g - \frac{1}{\tau_f \rho_g} \bar{\rho}_d (u'_g - u'_d) - \frac{1}{\tau_f \rho_g} \rho'_d (\bar{u}_g - \bar{u}_d), \quad (32)$$

$$-i\tilde{\omega}_g v'_g + w'_g \frac{d\bar{v}_g}{dz} = -\frac{1}{2} \Omega_K u'_g - \frac{1}{\tau_f \rho_g} \bar{\rho}_d (v'_g - v'_d) - \frac{1}{\tau_f \rho_g} \rho'_d (\bar{v}_g - \bar{v}_d), \quad (33)$$

$$-i\tilde{\omega}_g w'_g = -\frac{dP'}{dz} - \frac{1}{\tau_f \rho_g} \bar{\rho}_d (w'_g - w'_d). \quad (34)$$

$$-i\tilde{\omega}_d \rho'_d + ik \bar{\rho}_d u'_d + \bar{\rho}_d \frac{dw'_d}{dz} + \frac{d\bar{\rho}_d}{dz} w'_d = 0, \quad (35)$$

$$-i\tilde{\omega}_d u'_d + w'_d \frac{d\bar{u}_d}{dz} = 2\Omega_K v'_d - \frac{1}{\tau_f} (u'_d - u'_g), \quad (36)$$

$$-i\tilde{\omega}_d v'_d + w'_d \frac{d\bar{v}_d}{dz} = -\frac{1}{2} \Omega_K u'_d - \frac{1}{\tau_f} (v'_d - v'_g), \quad (37)$$

$$-i\tilde{\omega}_d w'_d = -\frac{1}{\tau_f} (w'_d - w'_g), \quad (38)$$

where $\tilde{\omega}_g = \omega - k\bar{u}_g$ and $\tilde{\omega}_d = \omega - k\bar{u}_d$.

4.2. Energy Equations

We consider the radial energy budget for gas. Multiplying equation (32) by $u_g'^*$ yields

$$\begin{aligned} -i\tilde{\omega}_g|u_g'|^2 &= -\frac{d\bar{u}_g}{dz}w_g'u_g'^* - ik\frac{1}{\rho_g}P'u_g'^* + 2\Omega_K v_g'u_g'^* - \frac{1}{\tau_f\rho_g}\bar{\rho}_d(u_g' - u_d')u_g'^* \\ &\quad + \frac{1}{\tau_f\rho_g}(\bar{u}_g - \bar{u}_d)\rho_d'u_g'^*, \end{aligned} \quad (39)$$

where the superscript * denotes the complex conjugate. Taking the real part yields

$$\begin{aligned} \omega_I|u_g'|^2 &= -\frac{d\bar{u}_g}{dz}\Re[w_g'u_g'^*] + k\frac{1}{\rho_g}\Im[P'u_g'^*] + 2\Omega_K\Re[v_g'u_g'^*] - \frac{1}{\tau_f\rho_g}\bar{\rho}_d\Re[(u_g' - u_d')u_g'^*] \\ &\quad - \frac{1}{\tau_f\rho_g}(\bar{u}_g - \bar{u}_d)\Re[\rho_d'u_g'^*]. \end{aligned} \quad (40)$$

We perform the similar manipulations for azimuthal and vertical directions,

$$\begin{aligned} \omega_I|v_g'|^2 &= -\frac{d\bar{v}_g}{dz}\Re[w_g'v_g'^*] + 2\Omega_K\Re[u_g'v_g'^*] - \frac{1}{\tau_f\rho_g}\bar{\rho}_d\Re[(v_g' - v_d')v_g'^*] \\ &\quad - \frac{1}{\tau_f\rho_g}(\bar{v}_g - \bar{v}_d)\Re[\rho_d'v_g'^*], \end{aligned} \quad (41)$$

$$\omega_I|w_g'|^2 = -\frac{1}{\rho_g}\Re\left[\frac{dP'}{dz}w_g'^*\right] - \frac{1}{\tau_f\rho_g}\bar{\rho}_d\Re[(w_g' - w_d')w_g'^*] - \frac{1}{\tau_f\rho_g}(\bar{w}_g - \bar{w}_d)\Re[\rho_d'w_g'^*]. \quad (42)$$

Similarly, we consider the energy budgets for dust.

$$\omega_I|u_d'|^2 = -\frac{d\bar{u}_d}{dz}\Re[w_d'u_d'^*] + 2\Omega_K\Re[v_d'u_d'^*] - \frac{1}{\tau_f}\Re[(u_d' - u_g')u_d'^*], \quad (43)$$

$$\omega_I|v_d'|^2 = -\frac{d\bar{v}_d}{dz}\Re[w_d'v_d'^*] - \frac{1}{2}\Omega_K\Re[u_d'v_d'^*] - \frac{1}{\tau_f}\Re[(v_d' - v_g')v_d'^*], \quad (44)$$

$$\omega_I|w_d'|^2 = -\frac{1}{\tau_f}\Re[(w_d' - w_g')w_d'^*]. \quad (45)$$

Here, let us see the total energy budget. Multiplying equations (40)–(42) by ρ_g and equations (43)–(45) by $\bar{\rho}_d$, we sum them. Note that equations (41), (44) is multiplied by 4 in order to eliminate Epicyclic terms.

$$\begin{aligned} &\omega_I\{\rho_g(|u_g'|^2 + 4|u_g'v_g'|^2 + |u_g'w_g'|^2) + \bar{\rho}_d(|u_d'|^2 + 4|u_d'v_d'|^2 + |u_d'w_d'|^2)\} \\ &= -\left\{\frac{d\bar{u}_g}{dz}\Re[w_g'u_g'^*] + \frac{d\bar{u}_d}{dz}\Re[w_d'u_d'^*] + 4\frac{d\bar{v}_g}{dz}\Re[w_g'v_g'^*] + 4\frac{d\bar{v}_d}{dz}\Re[w_d'v_d'^*]\right\} \\ &\quad -\Re\left[ikP'u_g'^* + \frac{dP'}{dz}w_g'^*\right] - \frac{\bar{\rho}_d}{\tau_f}\{|u_g' - u_d'|^2 + 4|v_g' - v_d'|^2 + |w_g' - w_d'|^2\} \\ &\quad - \frac{1}{\tau_f}\{(\bar{u}_g - \bar{u}_d)\Re[\rho_d'u_g'^*] + 4(\bar{v}_g - \bar{v}_d)\Re[\rho_d'v_g'^*]\}. \end{aligned} \quad (46)$$

The equation (46) is integrated in the z -direction in order to examine the total energy budget. We focus on the pressure term of the second term of the right hand in the equation (46).

$$\int \frac{dP'}{dz} w_g'^* dz = - \int P' \left(\frac{dw_g'}{dz} \right)^* dz = - \int P' i k u_g'^* dz, \quad (47)$$

where the partial integration and the periodic boundary condition are used in the first equality, and the equation (31) is used in the second equality. We have

$$\int \left(P' i k u_g'^* + \frac{dP'}{dz} w_g'^* \right) dz = 0. \quad (48)$$

Thus, the total energy budget of the system is determined by the shear terms, the friction terms due to the fluctuation of the dust density, and the frictional dissipation terms; the total energy does not change by the pressure terms and epicyclic terms, and they merely exchange energy among x , y , and z directions. Figure 7 shows the each term in energy equations (40)–(45) and Figure 8 shows the each term in total energy equation (46) for $k\eta r = 10.8$ at which the growth rate has maximum value for $\tau_f \Omega_K = 1$ and $\rho_d(0)/\rho_g = 1$. Then the shear of radial and azimuthal velocities of gas is a main energy source.

Figure 9 shows the each term in energy equations (40)–(45) and Figure 10 shows the each term in total energy equation (46) for $k\eta r = 48.6$ at which the growth rate has maximum value for $\tau_f \Omega_K = 10^{-3}$ and $\rho_d(0)/\rho_g = 1$. The shears of azimuthal velocities $d\bar{v}_g/dz$ and $d\bar{v}_d/dz$ are main energy sources. In addition, the radial relative velocity between dust and gas, coupled with the density fluctuations, are also an important energy source.

In energy equation (46), the last term $-\frac{1}{\tau_f} \{(\bar{u}_g - \bar{u}_d)\Re[\rho_d' u_g'^*] + 4(\bar{v}_g - \bar{v}_d)\Re[\rho_d' v_g'^*]\}$ shows an instability powered by relative velocity of gas and dust, coupled with Eulerian dust density fluctuation. Substituting the linearized continuity equation for dust (35),

$$\rho_d' = -i \frac{\tilde{\omega}_d^*}{|\tilde{\omega}_d|^2} \left(i k \bar{\rho}_d u_d' + \bar{\rho}_d \frac{dw_d'}{dz} + \frac{d\bar{\rho}_d}{dz} w_d' \right), \quad (49)$$

this term is divided into parts

$$\begin{aligned} & -\frac{1}{\tau_f} \{(\bar{u}_g - \bar{u}_d)\Re[\rho_d' u_g'^*] + 4(\bar{v}_g - \bar{v}_d)\Re[\rho_d' v_g'^*]\} \\ = & -\frac{1}{\tau_f} \frac{1}{|\tilde{\omega}_d|^2} \bar{\rho}_d \left\{ (\bar{u}_g - \bar{u}_d)\Im \left[\tilde{\omega}_d^* \left(i k u_d' + \frac{dw_d'}{dz} \right) u_g'^* \right] + 4(\bar{v}_g - \bar{v}_d)\Im \left[\tilde{\omega}_d^* \left(i k u_d' + \frac{dw_d'}{dz} \right) v_g'^* \right] \right\} \\ & -\frac{1}{\tau_f} \frac{1}{|\tilde{\omega}_d|^2} \frac{d\bar{\rho}_d}{dz} \{(\bar{u}_g - \bar{u}_d)\Im[\tilde{\omega}_d^* w_d' u_g'^*] + 4(\bar{v}_g - \bar{v}_d)\Im[\tilde{\omega}_d^* w_d' v_g'^*]\}. \end{aligned} \quad (50)$$

The first term in the right hand of equation (50) presumably corresponds to the streaming instability addressed by Youdin & Goodman (2005), Youdin & Johansen (2007) and Johansen & Youdin (2007). The divergence of the dust velocity $\left(i k u_d' + \frac{dw_d'}{dz} \right)$ denotes that the increase of the fluctuation of dust density is related to the streaming instability. If $\rho_g \gg \rho_d$ and $\tau_f \Omega_K \ll 1$, the

divergence of the dust velocity approaches zero owing to the incompressibility of gas and a small relative velocity between dust and gas. Thus, if dust size is small, the contribution of the first term of the right hand side of equation (50) to the instability becomes small. This is consistent with the results of Youdin & Goodman (2005) and Youdin & Johansen (2007). The second term on the right hand of equation (50) also denotes the power due to the fluctuation of dust density. However, the dust density fluctuation is produced by the vertical advection under the condition with an initial vertical dust density gradient. The fluctuation of dust density is the cause of instability in either term of the equation (50). The first term arises due to the Lagrangian density fluctuation. On the other hand, the cause of the density fluctuation is advection in the second term. The growth rate of instability ω_I and the phase velocity $v_p = \omega_R/k$ are estimated from the numerical result. Figure 11 shows each term on the left hand of equation (50) for $\tau_f \Omega_K = 10^{-3}$, $\rho_d(0)/\rho_g = 1$ and $h_d/z_d = 0.5$. Obviously, the energy is gained from the second term associated with Eulerian density fluctuation.

Because Youdin & Goodman (2005) and Youdin & Johansen (2007) have assumed that dust density is constant, the instability caused by the second term in the equation (50) has not been seen. In a density stratified layer, if the dust size is small, the instability which obtains the energy through the second term in addition to the shear terms occurs.

Let us see the relation between the two-fluid instability and the baroclinic instability stated in Ishitsu & Sekiya (2003). One fluid approximation assumes infinitesimal friction time $\tau_f \rightarrow 0$. In order for the friction term in equations (11) and (13) to be finite, we have $\mathbf{u}_g \rightarrow \mathbf{u}_d$. Eliminating the friction terms by adding equation (11) $\times (\rho_g/\rho)$ and equation (13) $\times (\rho_d/\rho)$ where $\rho \equiv \rho_g + \rho_d$, we have

$$\frac{\partial \mathbf{u}}{\partial t} + (\mathbf{u} \cdot \nabla_2) \mathbf{u} = -\frac{1}{\rho} \nabla_2 P + 2\mathbf{u} \times \boldsymbol{\Omega}_K + \frac{3}{2} u \Omega_K \hat{\mathbf{y}}, \quad (51)$$

where $\mathbf{u} \equiv \mathbf{u}_g = \mathbf{u}_d$. Linearizing the pressure term in the equation (51) yields

$$-\frac{1}{\bar{\rho} + \rho'} \frac{\partial(\bar{P} + P')}{\partial r} \approx -\frac{1}{\bar{\rho}} \frac{\partial P'}{\partial r} + \frac{1}{\bar{\rho}^2} \frac{\partial \bar{P}}{\partial r} \rho'. \quad (52)$$

The second term in the right hand is the buoyancy term, which is the cause of the baroclinic instability for the one-fluid approximation (Ishitsu & Sekiya 2002). Note that we assume the gas to be incompressible. In the one-fluid model, the fluid of dust and gas mixture is also incompressible because $\nabla \cdot \mathbf{u} = \nabla \cdot \mathbf{u}_g = 0$. Thus, the dust density perturbation arises not from the compression but from the advection; the latter can have non-zero value if $\nabla \bar{\rho} \neq 0$. Adding equation (24) by $\rho_g/\bar{\rho}$ and equation (28) by $\bar{\rho}_d/\bar{\rho}$, we have

$$\begin{aligned} & \frac{\partial}{\partial t} \left(\frac{\rho_g u'_g + \bar{\rho}_d u'_d}{\bar{\rho}} \right) + \frac{\rho_g \bar{u}_g}{\bar{\rho}} \frac{\partial u'_g}{\partial x} + \frac{\bar{\rho}_d \bar{u}_d}{\bar{\rho}} \frac{\partial u'_d}{\partial x} + \frac{\rho_g w'_g}{\bar{\rho}} \frac{\partial \bar{u}_g}{\partial z} + \frac{\bar{\rho}_d w'_g}{\bar{\rho}} \frac{\partial \bar{u}_d}{\partial z} \\ &= -\frac{1}{\bar{\rho}} \frac{\partial P'}{\partial z} + 2\Omega_K \frac{\rho_g v'_g + \bar{\rho}_d v'_d}{\bar{\rho}} - \frac{\rho'_d}{\tau_f \bar{\rho}} (\bar{u}_g - \bar{u}_d). \end{aligned} \quad (53)$$

It is easily seen that the left hand side and the Coriolis force term in the right hand side become those of the linearized equation of equations (51) in the limit $\mathbf{u}_g \rightarrow \mathbf{u}_d$. We see the frictional term

in the right hand of the equation (53) is written

$$\begin{aligned}
 -\frac{1}{\tau_f \bar{\rho}}(\bar{u}_g - \bar{u}_d)\rho'_d &= -\frac{1}{\tau_f \bar{\rho}} \frac{2(\rho_g + \bar{\rho}_d)\rho_g \tau_f \Omega_K}{(\rho_g + \bar{\rho}_d)^2 + (\rho_g \tau_f \Omega_K)^2} \eta v_K \rho'_d \\
 &= \frac{1}{\bar{\rho}} \frac{\rho_g + \bar{\rho}_d}{(\rho_g + \bar{\rho}_d)^2 + (\rho_g \tau_f \Omega_K)^2} \frac{\partial P}{\partial r} \rho'_d,
 \end{aligned} \tag{54}$$

where we use equations (9), (17), and (19). Limiting to the one-fluid leads

$$-\frac{1}{\tau_f \rho_g}(\bar{u}_g - \bar{u}_d)\rho'_d \rightarrow \frac{1}{\bar{\rho}^2} \frac{\partial P}{\partial r} \rho'_d \quad \text{as } \tau_f \rightarrow 0. \tag{55}$$

This term corresponds to the second term in the right hand of the equation (52). However, two-fluid instability is different from the baroclinic instability with regards that the baroclinic instability has no axis-symmetric mode.

5. Conclusions

We performed the two-fluid of gas and dust, two-dimensional simulations in the dust layer of a protoplanetary disk. For $\tau_f \Omega_K = 10^{-3}$, the numerical simulations show the rapid growth instability induced mainly by the vertical shear of azimuthal velocity, and additionally the relative motion between dust and gas coupled with the dust density fluctuation due to advection if the dust density distribution has significant gradient, $|\frac{d\rho_d}{dz}| \gtrsim \rho_d(0)/\eta r$. The streaming instability stated by Youdin & Johansen (2007), which is caused by the relative motion of dust and gas coupled with the Lagrangian dust density fluctuation, has the small growth rate of the instability if the dust size is smaller than several centimeters. On the other hand, the instability powered by the vertical shear of the azimuthal velocity, and additionally by the relative velocity of dust and gas coupled with dust density fluctuation due to advection shown in this work has the growth rate Ω_K even if the dust size is small.

The density fluctuations grows due to the streaming instability if the initial dust density is constant, which is accompanied by the concentrations of dust density. However, if the initial dust density is not constant, the instability related by the vertical dust density gradient occurs. The latter instability diffuses the dust rather than concentrates that. This suggests that the maximum density does not always increase from the initial value.

Additionally, for $\tau_f \Omega_K = 1$, the simulations shows the vertical shear of the radial flow plays the important role. After the flow becomes a turbulent state due to the shear instability, the dust concentrations are induced by the streaming instability because large relative motion between dust and gas is permissible due to loose coupling of dust and gas.

Chiang (2008) and Barranco (2009) have performed the one-fluid, 3D simulations of the shear instability and presented that the conditions of the transition to turbulence depends not only on the Richardson number but also on the initial perturbations. The dependency of the shear instability

on initial conditions is explained as follows. The growth rate of the instability depends on the radial and the azimuthal wave numbers k_r and k_ϕ if there is no the radial shear such as the Kepler shear. The unstable region in the Fourier space is restricted to a small value of k_r (see figure 1 in Ishitsu & Sekiya (2003)). In addition, the shear instability does not have the axis-symmetric unstable mode, that is, $k_\phi = 0$ mode. If there is radial shear due to the Kepler motion, the radial wave number increases due to shear-stretching as time passes (see equation (43) in Ishitsu & Sekiya (2003)),

$$k_r(t) = k_r(0) + \frac{3}{2}k_\phi t\Omega_K. \quad (56)$$

The perturbation can grow only when its wave number passes the unstable region in the Fourier space. The flow can transit into turbulence due to the transient amplification if the initial perturbation is large. On the other hand, the flow cannot transit into turbulence for small values of initial perturbations.

However, the instability of two-fluid shown in this work has the axis-symmetric unstable mode. As a result, the stabilization caused by the increase of the azimuthal wave number due to the radial shear is not effective. We expect that the instability occurs in the radial direction, and then the perturbation with small azimuthal wave number grows.

Chiang (2008) estimates the critical dust surface density as the condition that the shear instability does not occur if there is not a global turbulence such as MRI. This estimation is derived from one-fluid simulations. However, in two-fluid of gas and dust, the instability due to the vertical dust density gradient and the relative motion between gas and dust occurs. The flow can transit into turbulence even if the disk has the critical surface density estimated by Chiang (2008). Thus, the instability induced by the dust density gradient may preclude the planetesimal formation due to the gravitational instability.

In the field of the meteoritics, 1 Myr time-lag between the formations of Calcium-Aluminum rich inclusions (CAI) and chondrule is known (Scott 2006). If the most of planetesimals are formed of chondrules, dust aggregates as precursors of chondrules need to be retained in a disk during 1 Myr. However, the gas friction makes the mm-sized dust in a laminar disk to fall within 0.1Myr. If the disk is turbulent, some of the dust may avoid falling due to the turbulent diffusion. Thus, even though the global turbulence is weak in the dead zone, the turbulence due to the instability described in this paper may play the role of avoiding planetesimal formation and floating dust in the disk.

The instability induced by the relative motion between gas and dust should be studied more detailedly because this instability have possible important roles in the dust evolution and the planetesimal formation in the protoplanetary disk.

The calculations in this work were partly performed with computers at Astronomical Data Analysis Center, National Astronomical Observatory of Japan. This work was supported by Ministry of Education, Culture, Sports, Science and Technology of Japan (MEXT) Grant-in-Aid for

Scientific Research on Priority Areas, “Development of Extrasolar Planetary Science” (MEXT-16077202).

REFERENCES

- Adachi, I., Hayashi, C., & Nakazawa, K. 1976, *Progress of Theoretical Physics*, 56, 1756
- Balbus, S. A., & Hawley, J. F. 1991, *ApJ*, 376, 214
- Barranco, J. A. 2009, *ApJ*, 691, 907
- Canuto, C. et al. 1988, *Spectral methods in fluid dynamics* (Springer-Verlag)
- Chiang, E. 2008, *ApJ*, 675, 1549
- Coradini, A., Magni, G., & Federico, C. 1981, *A&A*, 98, 173
- Cuzzi, J. N., Dobrovolskis, A. R., & Champney, J. M. 1993, *Icarus*, 106, 102
- Dobrovolskis, A. R., Dacles-Mariani, J. S., & Cuzzi, J. N. 1999, *J. Geophys. Res.*, 104, 30805
- Epstein, P. S. 1924, *Physical Review*, 23, 710
- Goldreich, P. & Ward, W. R. 1973, *ApJ*, 183, 1051
- Garaud, P., & Lin, D. N. C. 2004, *ApJ*, 608, 1050
- Hayashi, C. 1981, , *Progress of Theoretical Physics*, 70, 35
- Hayashi, C., Nakazawa, K., & Nakagawa, Y. 1985, *Protostars and Planets II*, 1100
- Ishitsu, N. & Sekiya, M. 2002, *Earth, Planets, and Space*, 54, 917
- Ishitsu, N. & Sekiya, M. 2003, *Icarus*, 165, 181
- Johansen, A., Klahr, H., & Henning, T. 2006a, *ApJ*, 636, 1121
- Johansen, A., Henning, T., & Klahr, H. 2006b, *ApJ*, 643, 1219
- Johansen, A., & Youdin, A. 2007, *ApJ*, 662, 627
- Johansen, A., Oishi, J. S., Low, M.-M. M., Klahr, H., Henning, T., & Youdin, A. 2007, *Nature*, 448, 1022
- Kornet, K., Stepinski, T. F., & Różyczka, M. 2001, *A&A*, 378, 180
- Landau, L. D., & Lifshits, E. M. 1987, *Fluid Mechanics*; 2nd ed (Oxford: Butterworth-Heinemann)
- Michikoshi, S., & Inutsuka, S.-i. 2006, *ApJ*, 641, 1131

- Nakagawa, Y., Sekiya, M., & Hayashi, C. 1986, *Icarus*, 67, 375
- Safroov, V. S. 1969, *Evolution of the Protoplanetary Cloud and Formation of the Earth and the Planets* (NASA Tech. Trans. F-677; Moscow: Nauka Press)
- Sano, T., Miyama, S. M., Umebayashi, T., & Nakano, T. 2000, *ApJ*, 543, 486
- Sekiya, M. 1983, *Progress of Theoretical Physics*, 69, 1116
- Sekiya, M. 1998, *Icarus*, 133, 298
- Sekiya, M. & Ishitsu, N. 2000, *Earth, Planets, and Space*, 52, 517
- Sekiya, M. & Ishitsu, N. 2001, *Earth, Planets, and Space*, 53, 761
- Scott, E. R. D. 2006, *Icarus*, 185, 72
- Youdin, A. N., & Goodman, J. 2005, *ApJ*, 620, 459
- Youdin, A., & Johansen, A. 2007, *ApJ*, 662, 613
- Wakita, S., & Sekiya, M. 2008, *ApJ*, 675, 1559
- Weidenschilling, S. J. 1977, *MNRAS*, 180, 57
- Weidenschilling, S. J. 1980, *Icarus*, 44, 172
- Weidenschilling, S. J., & Cuzzi, J. N. 1993, *Protostars and Planets III*, 1031
- Wurm, G., Blum, J., & Colwell, J. E. 2001, *Icarus*, 151, 318
- Yamoto, F., & Sekiya, M. 2004, *Icarus*, 170, 180

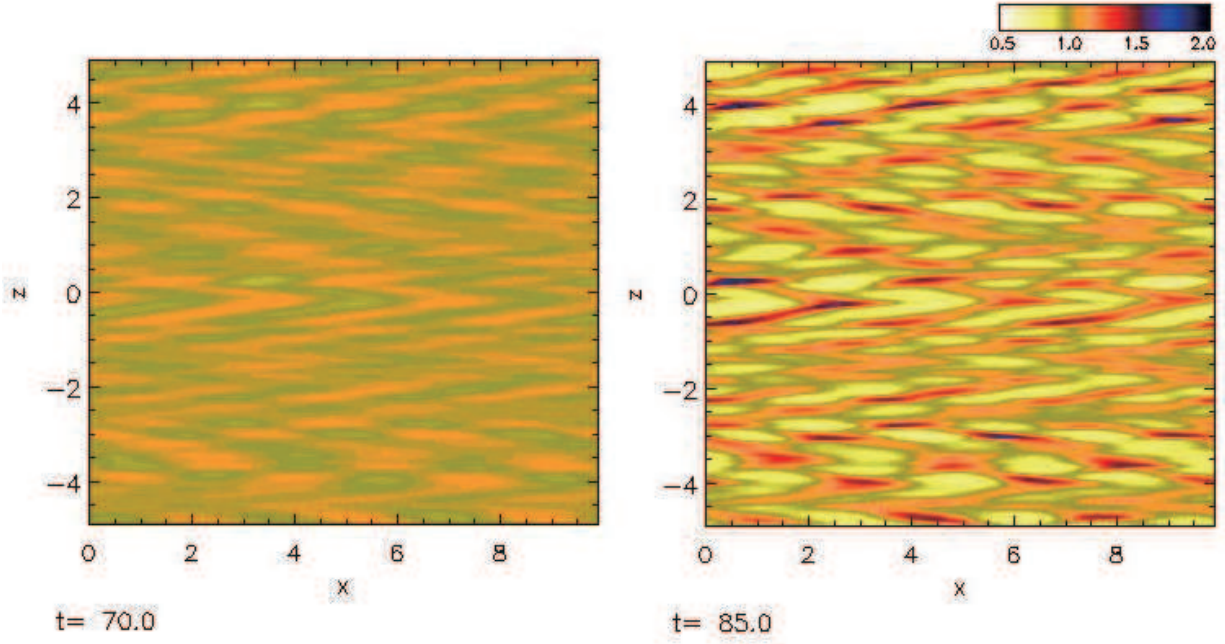


Fig. 1.— Snapshots of dust density at times $t\Omega_K = 70$ and 85, in the case where $\tau_f\Omega_K = 1$ and $\rho_d(0)/\rho_g = 1$. Time, length and density are normalized by $\Omega_K, \eta r$ and ρ_g , respectively.

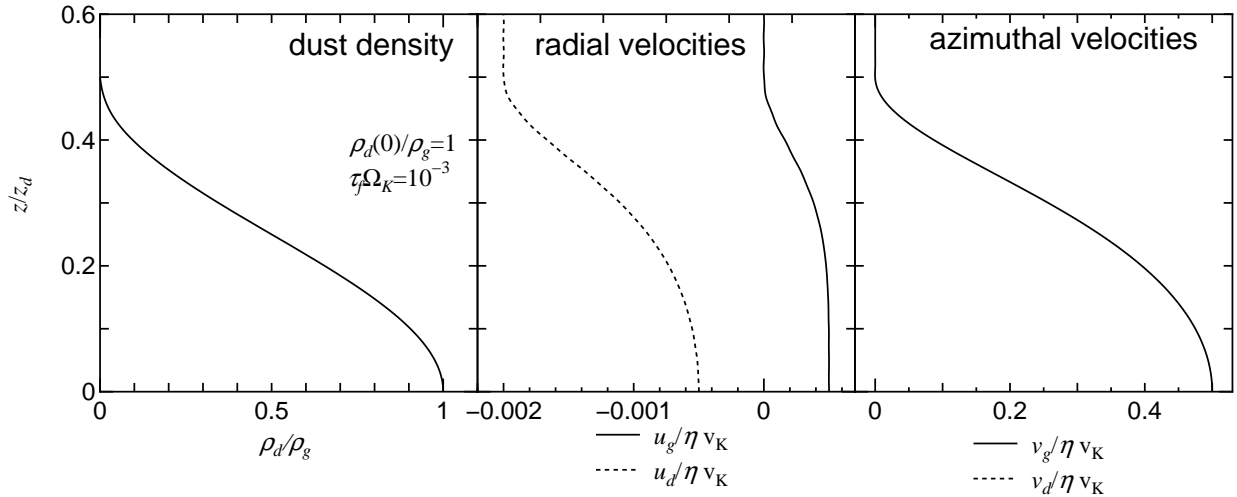


Fig. 2.— Distributions of dust density, gas and dust velocities of the initial flow in the case where $\tau_f\Omega_K = 10^{-3}$ and $\rho_d(0)/\rho_g = 1$. In the right panel, the curve of the dust velocity is not seen because the gas and dust have the almost same azimuthal velocity.

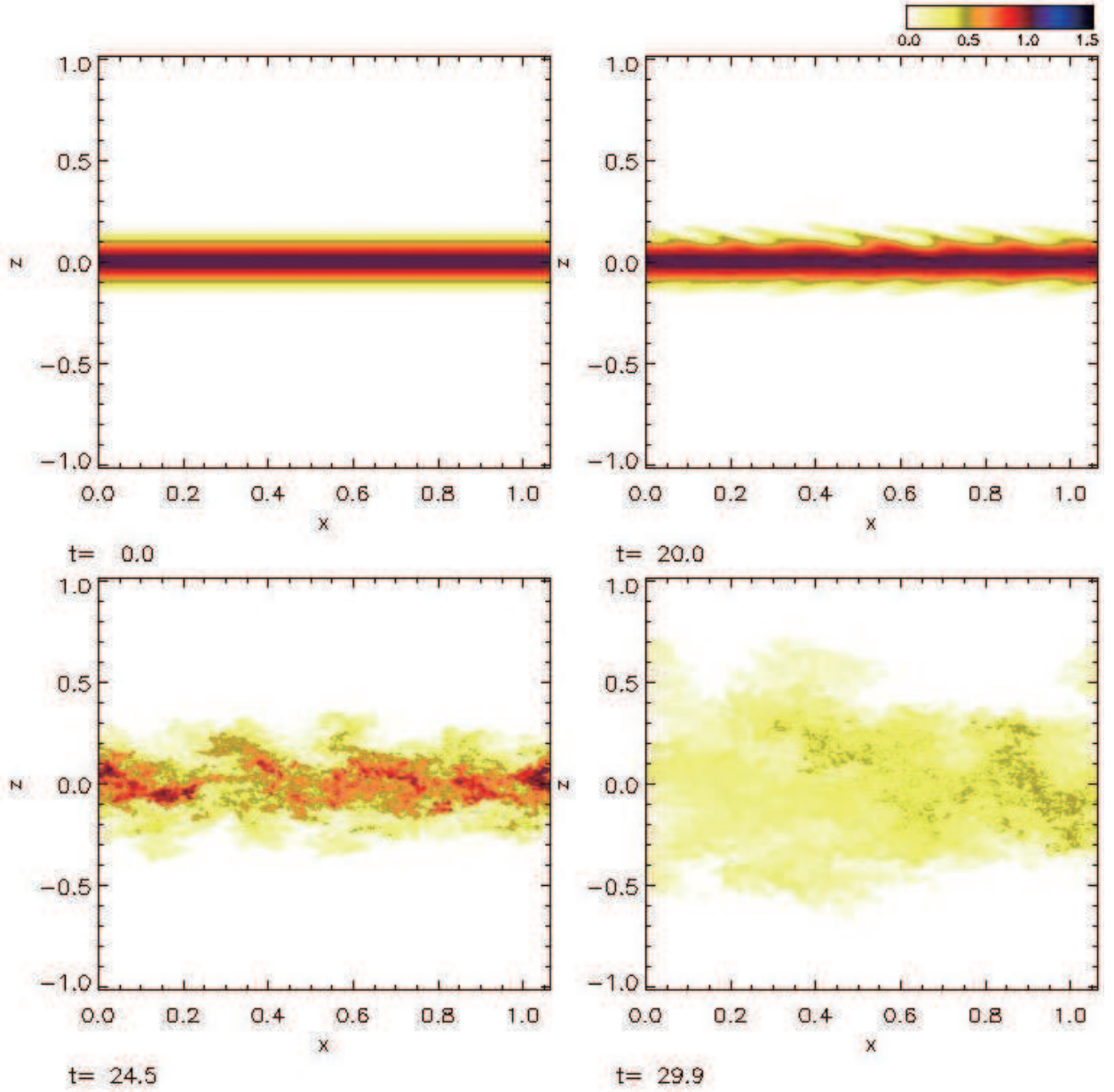


Fig. 3.— Snapshots of dust density at times $t\Omega_K = 0, 20.0, 24.5$ and 29.9 , in the case where $\tau_f\Omega_K = 10^{-3}$ and $\rho_d(0)/\rho_g = 1$.

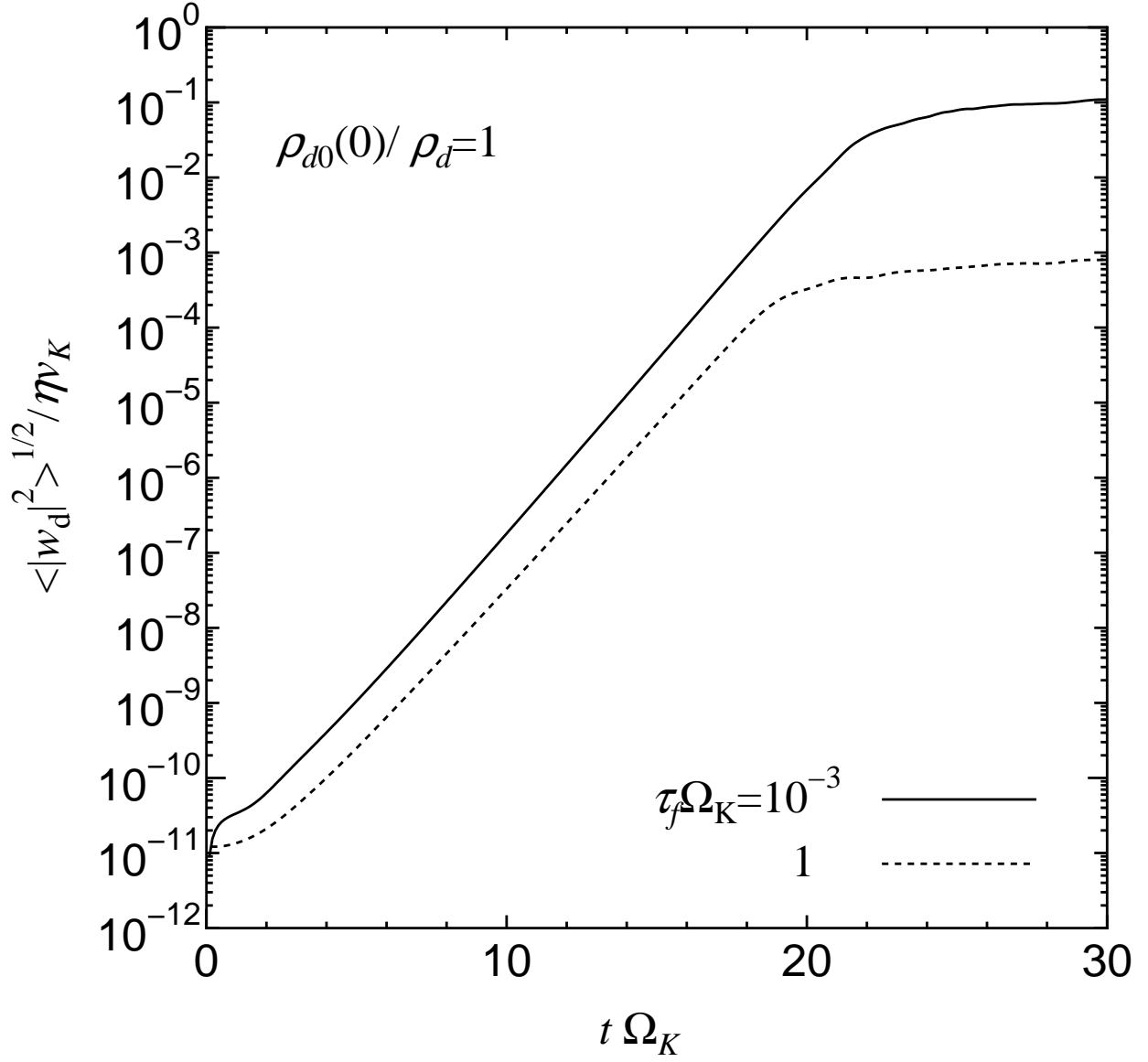


Fig. 4.— The time evolutions of the density weighted average of the vertical dust r.m.s. defined by the equation (22), in the case where $\tau_f \Omega_K = 10^{-3}$ (solid) and 1 (dotted) with $\rho_d(0) / \rho_g = 1$.

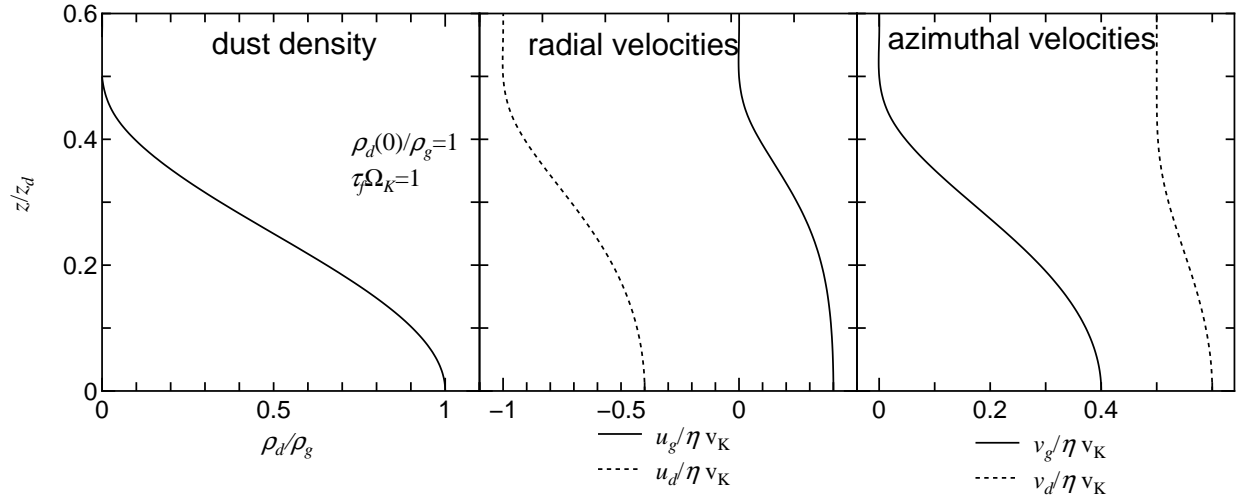


Fig. 5.— Distributions of dust density, gas and dust velocities of the initial flow in the case where $\tau_f \Omega_K = 1$ and $\rho_d(0)/\rho_g = 1$.

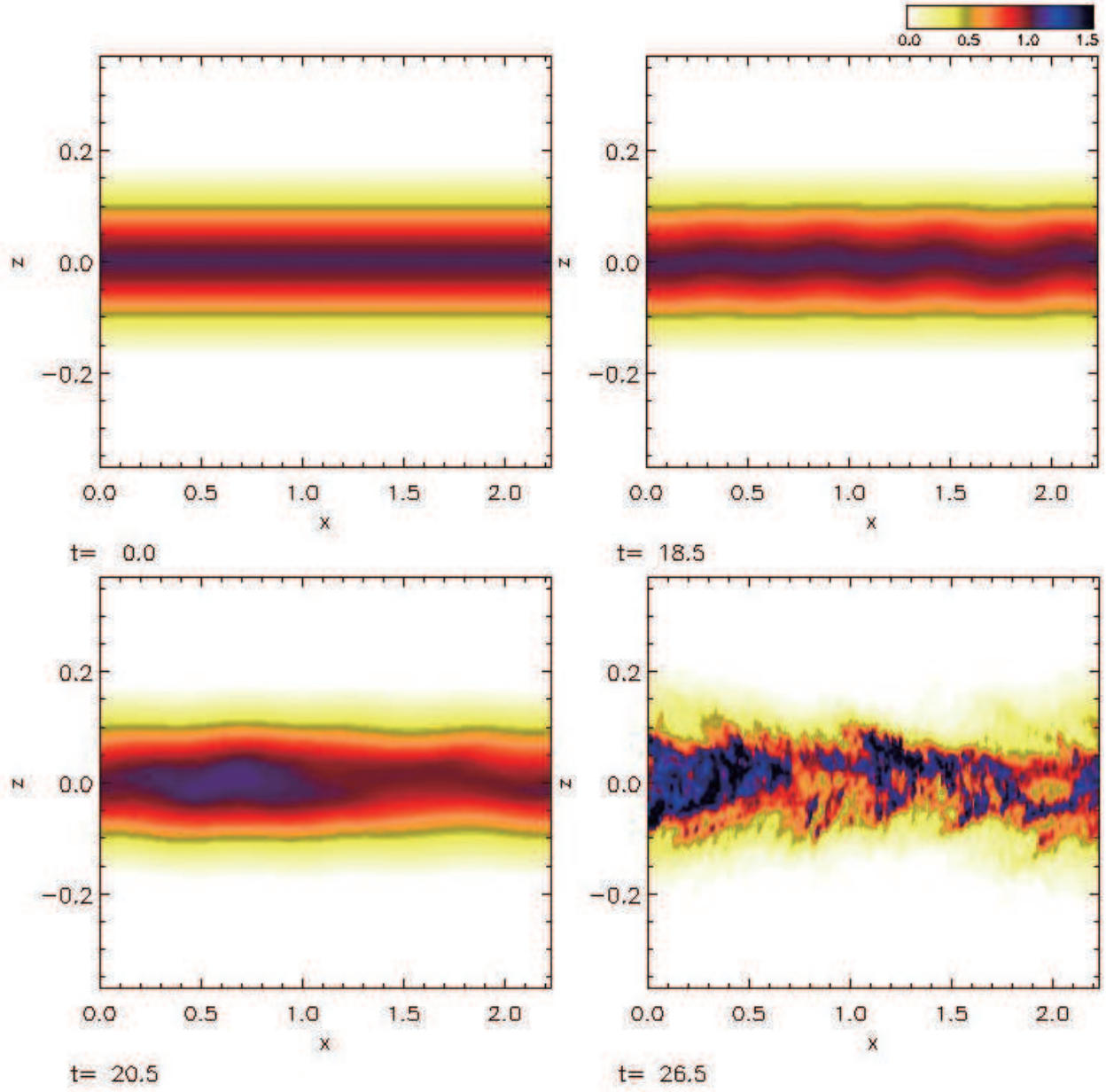


Fig. 6.— Snapshots of dust density at times $t\Omega_K = 0, 18.5, 20.5$ and 26.5 , in the case where $\tau_f\Omega_K = 1$ and $\rho_d(0)/\rho_g = 1$.

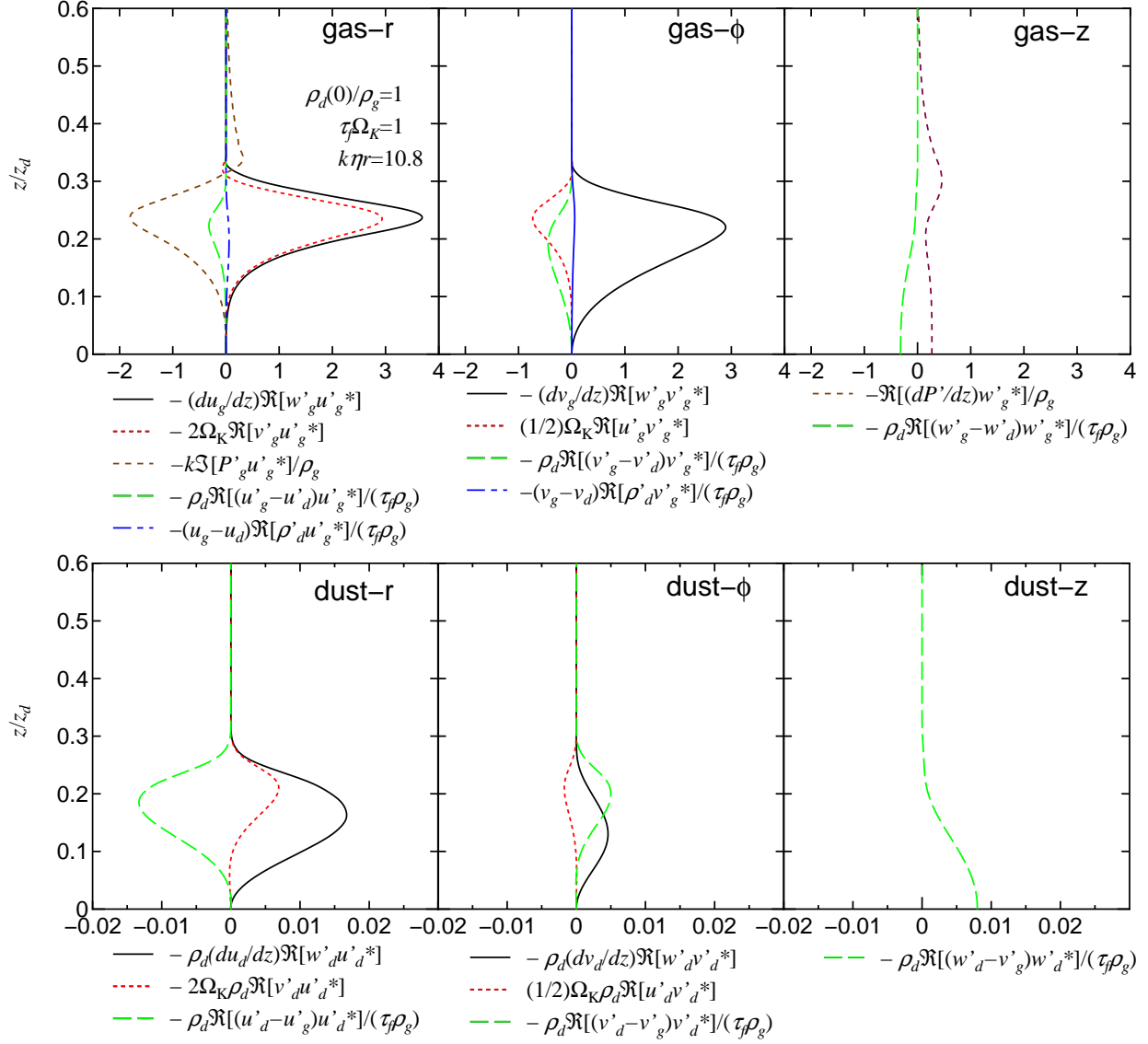


Fig. 7.— Each term in the right side of energy equations (40)–(45), in the case where $k\eta r = 10.8$, $\tau_f\Omega_K = 1$ and $\rho_d(0)/\rho_g = 1$.

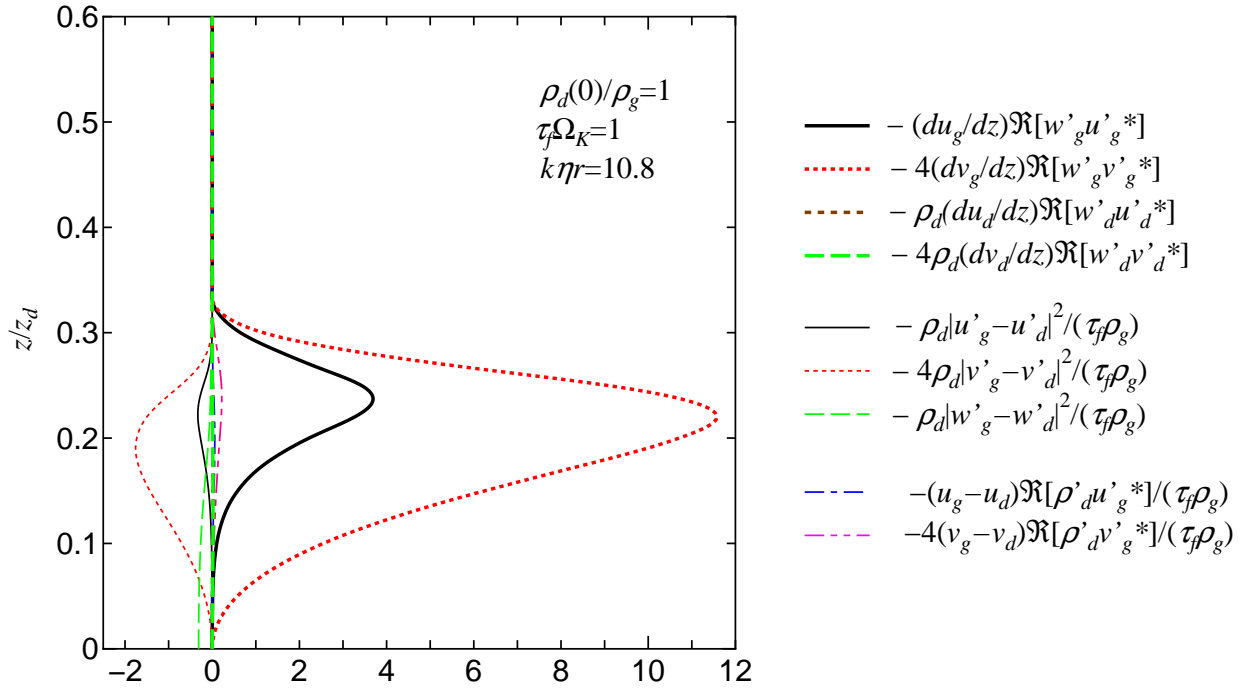


Fig. 8.— Each term in the right side of energy equation (46), in the case where $k\eta r = 10.8$, $\tau_f\Omega_K = 1$ and $\rho_d(0)/\rho_g = 1$.

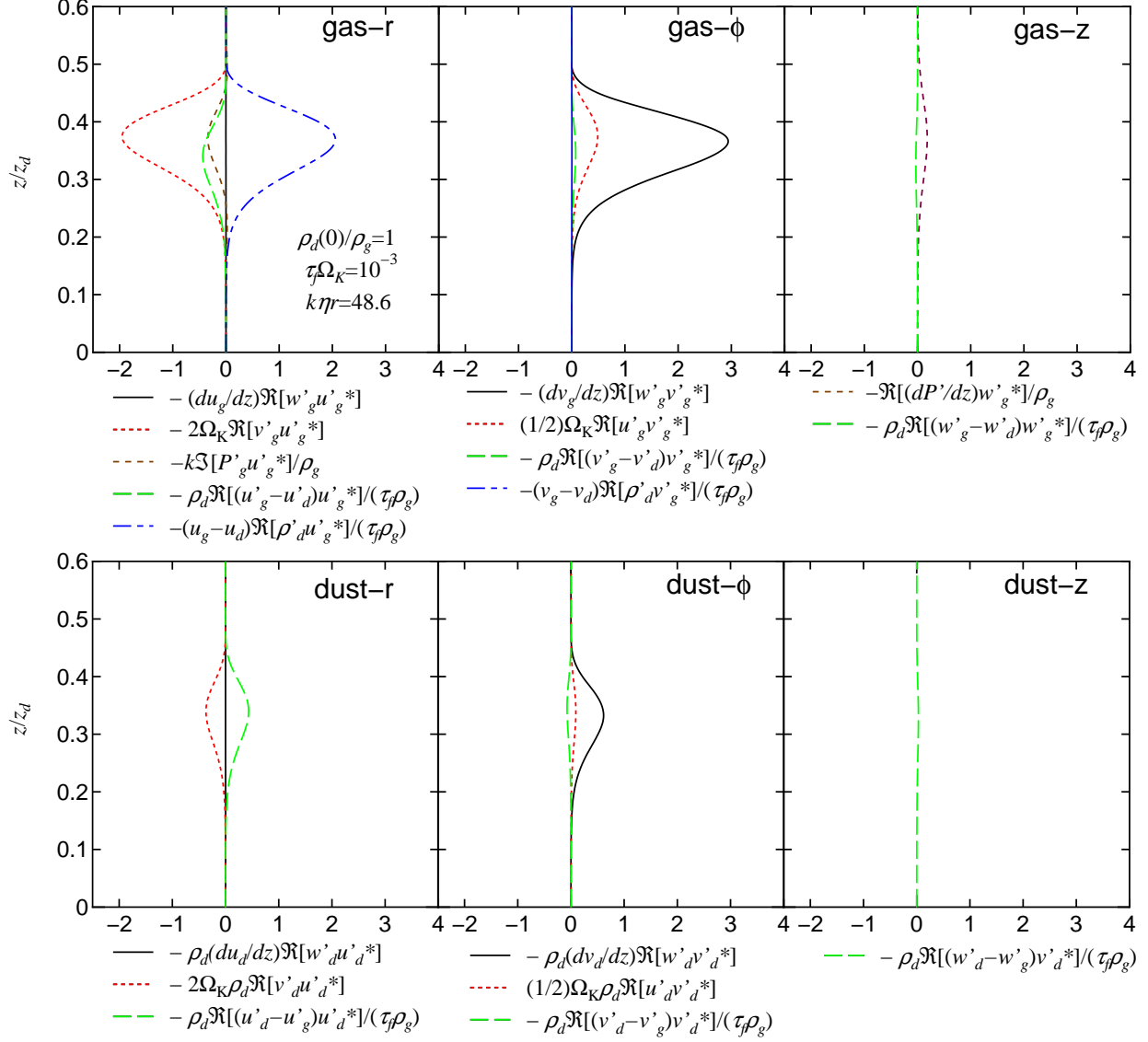


Fig. 9.— Each term in the right side of energy equations (40)–(45), in the case where $k\eta r = 48.6$, $\tau_f\Omega_K = 10^{-3}$ and $\rho_d(0)/\rho_g = 1$.

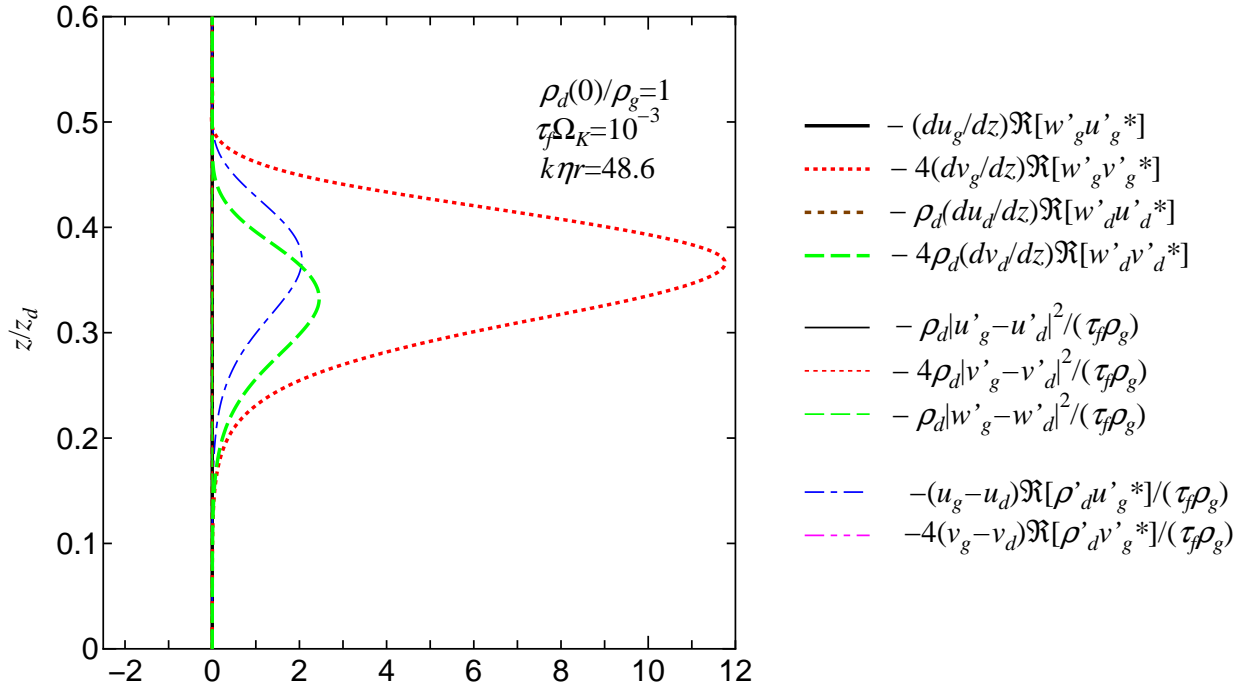


Fig. 10.— Each term in the right side of energy equation (46), in the case where $k\eta r = 48.6$, $\tau_f \Omega_K = 10^{-3}$ and $\rho_d(0)/\rho_g = 1$.

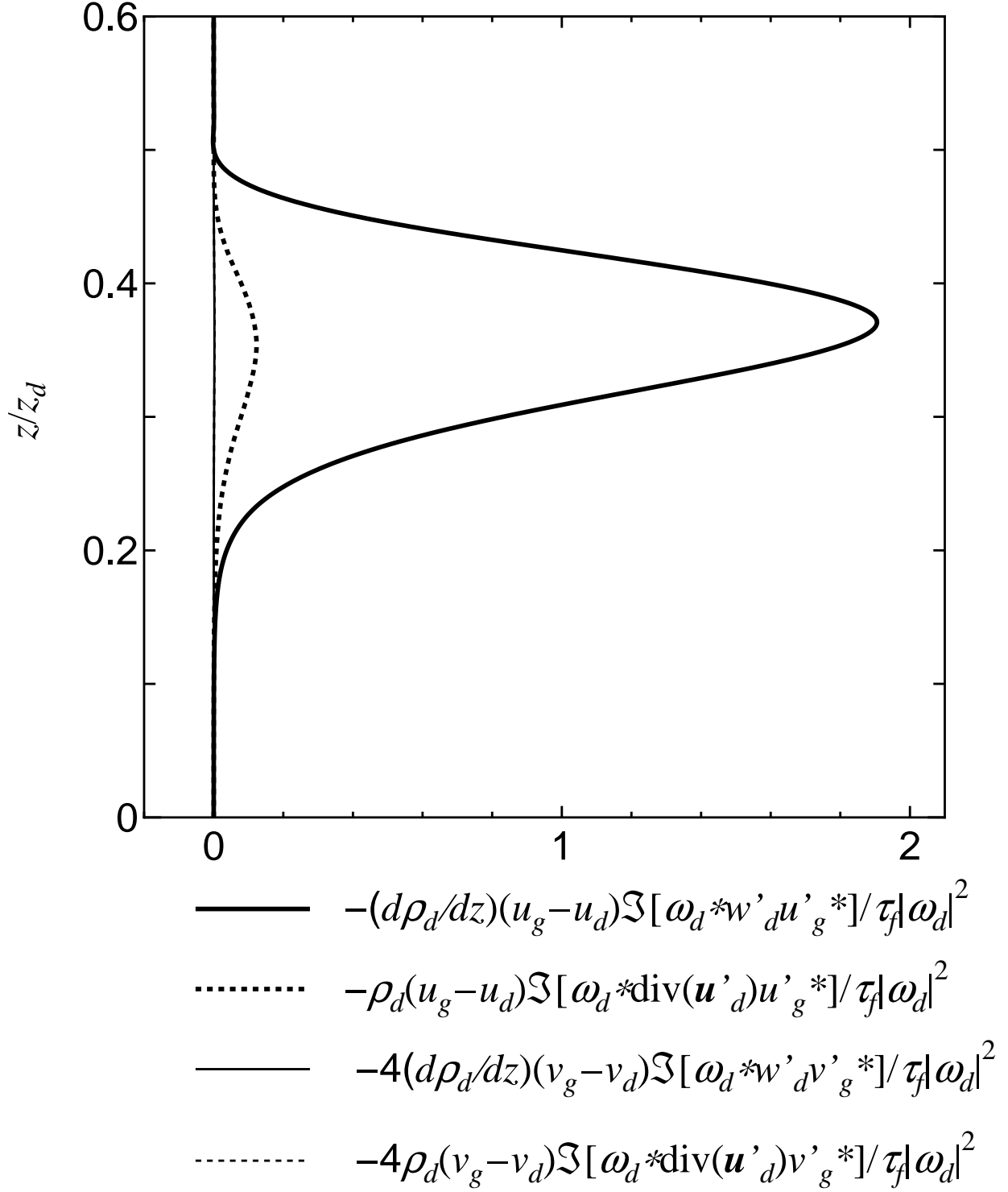


Fig. 11.— Each term in the right side of energy equation (50), in the case where $k\eta r = 48.6$, $\tau_f \Omega_K = 10^{-3}$ and $\rho_d(0)/\rho_g = 1$.

Table 1. Parameters and results

run	$\rho_d(0)/\rho_g$	h_d/z_d	$\tau_f\Omega_K$	$N_X \times N_z$ ^a	L_x/z_d	L_y/z_d	$\delta t\Omega_K$	$\tau_D\Omega_K$ ^b	$k\eta r$	ω_I/Ω_K
const	1.0	0.0	1	256×256	π	1.0	5.e-4	10^3	1.9	0.12
rlt3	1.0	0.5	10^{-3}	256×256	2π	6.0	5.e-4	10^3	48.6	1.00
rlt0	1.0	0.5	1	256×256	2π	8.0	2.e-4	10^3	10.8	1.09

^aThe number of Fourier components

^b $\tau_D\Omega_K = z_d^2\Omega_K/\nu_D$